Title

Experimental Measurement of the Solid Particle Concentration in Geophysical Turbulent Gas-Particle Mixtures

Journal

Journal of Geophysical Research: Solid Earth, 123(5)

ISSN

2169-9313

Authors

Weit, A
Roche, O
Dubois, T
et al.

Publication Date

2018-05-01

DOI

10.1029/2018jb015530

Peer reviewed

Experimental Measurement of the Solid Particle Concentration in Geophysical Turbulent Gas-Particle Mixtures

A. Weit[1], O. Roche[1], T. Dubois[2], and M. Manga[3]

[1] Université Clermont Auvergne, CNRS, IRD, OPGC, Laboratoire Magmas et Volcans, Clermont-Ferrand, France, [2] Université Clermont Auvergne, CNRS, Laboratoire de Mathématiques Blaise Pascal, Clermont-Ferrand, France, [3] Department of Earth and Planetary Science, University of California, Berkeley, CA, USA

Correspondence to: A. Weit, a.weit@opgc.univ-bpclermont.fr

Abstract

Dilute gas-particle mixtures in which the particles are carried by the turbulent fluid are found in various geophysical contexts, from cold snow avalanches to hot pyroclastic density currents. Though previous studies suggest that such mixtures have maximum particle concentrations of a few volume percent, the dependence of this maximum concentration on the Reynolds number is unclear. We addressed this issue through laboratory experiments in a vertical pipe, where dilute gas-particle mixtures were created by injecting a turbulent air flow from below. Nearly monodisperse mixtures of glass beads of different grain sizes (77 to 1,550 µm) were used with varying bulk concentrations from 0.025 to 8 vol. %. To create quasi-static mixtures, the mean air velocity matched the terminal settling velocity for the grain sizes investigated. The maximum Reynolds numbers of the mixtures were ~10^4–10^6. The air pressure indicated full support of the particle weight at concentrations down to 0.025 vol. %. Above a critical particle concentration, at which all the particles were suspended, subsequent additional particles were not maintained in the mixture and led to the formation of clusters that settled downward in the pipe to form a dense fluidized bed. Maximum mean particle concentrations of the dilute mixtures increased from ~1 to ~2.8 vol. % and reached a plateau at increasing mixture Reynolds number. These results give insights into the maximum particle concentrations of geophysical turbulent gas-particle mixtures and may serve to constrain observations as well as the input and output data of models.

1 Introduction

Geophysical dilute turbulent gas-particle mixtures are common in nature and include snow surge avalanches (Köhler et al., 2016; Louge et al., 2011), dust storms (Goudie & Middleton, 2001), and volcanic mixtures of fragmented magmas in conduits, eruptive plumes, and pyroclastic density currents (Andrews & Manga, 2012; Anilkumar et al., 1993; Carazzo et al., 2008; Dufek, 2016). The solid phase concentration in these turbulent mixtures is important for the overall dynamics because it affects fluid turbulence (Cantero, Cantelli, et al., 2012) and controls the degree of coupling between

the gas and the particles as well as the intensity and the frequency of the particle interactions (e.g., Del Bello et al., 2017). Observations, models, and analog experiments indicate particle volumetric concentrations typically less than 0.1–1 vol. % in these geophysical mixtures (Breard et al., 2016; Neri et al., 2014; Shao & Dong, 2006; Turnbull & McElwaine, 2007).

One of the major interests in these turbulent mixtures is the variation of the flow dynamics with an increase in particle concentration and whether a maximum concentration can be carried by the turbulent gas. According to the model of Cantero, Cantelli, et al. (2012) and Cantero, Shringarpure, and Balachandar (2012), which addresses primarily the dynamics of turbidity currents, the solid phase concentration in fluid-particle mixtures is less than ≈1 vol. % since higher concentrations require excessive turbulent kinetic energy. This model shows that fluid turbulence is suppressed when the product of the Richardson number by the dimensionless particle settling velocity is above a threshold value, which increases with the Reynolds number (considering the shear velocity of the gravity current as the characteristic velocity). This finding suggests that turbulent gas-particle mixtures might also have a maximum critical concentration, a value yet to be determined.

Here we address this issue through laboratory experiments in which we investigated the maximum particle concentration in turbulent gas-particle mixtures in a vertical pipe as a function of the Reynolds number. We first review the literature on gas-particle pipe flows and describe the methodology and the experimental device we used. We then present our experimental results and examine the characteristics of the mixtures as a function of their particle concentrations. Finally, we discuss the origin of the maximum particle concentrations observed as well as possible implications for geophysical gas-particle flows.

2 Gas-Particle Flows in Vertical Pipes

The main characteristics of turbulent pipe flows we considered for designing our experimental device and analyzing our results are presented below. The turbulence of a pure fluid flow in a cylindrical pipe is characterized by the dimensionless Reynolds number defined as

$$Re = \frac{\rho U D}{\mu}, \qquad (1)$$

where ρ is the density of the fluid, U is the fluid mean velocity, D is the pipe diameter, and $\mu$is the dynamic viscosity of the fluid. In a cylindrical pipe, flows are considered laminar at Re < ~2,000, in the transitional regime between laminar and turbulent conditions at Re ~ 2,000–4,000, and fully turbulent at Re > ~4,000 (Davidson, 2015). The mean velocity profile of the turbulent flow is characterized by a linear profile in the viscous sublayer and obeys the well-known logarithmic law in the core region (see supporting information and Tennekes & Lumley, 1972, for instance). In the vertical

cross-sectional view of the flow, the profile shows a nearly constant velocity over a wide central plateau and lower velocities at the boundary layers, which are thinner than in case of laminar flows (Figure 1). Fluctuations in turbulent flows are due to the presence of eddies, whose sizes are controlled by the size of the pipe, with the largest eddies being of the order of $D/2$. Eddy size decreases according to the principal of energy cascade down to the Kolmogorov length scale:

$$\eta \sim Re^{-3/4} D, \qquad (2)$$

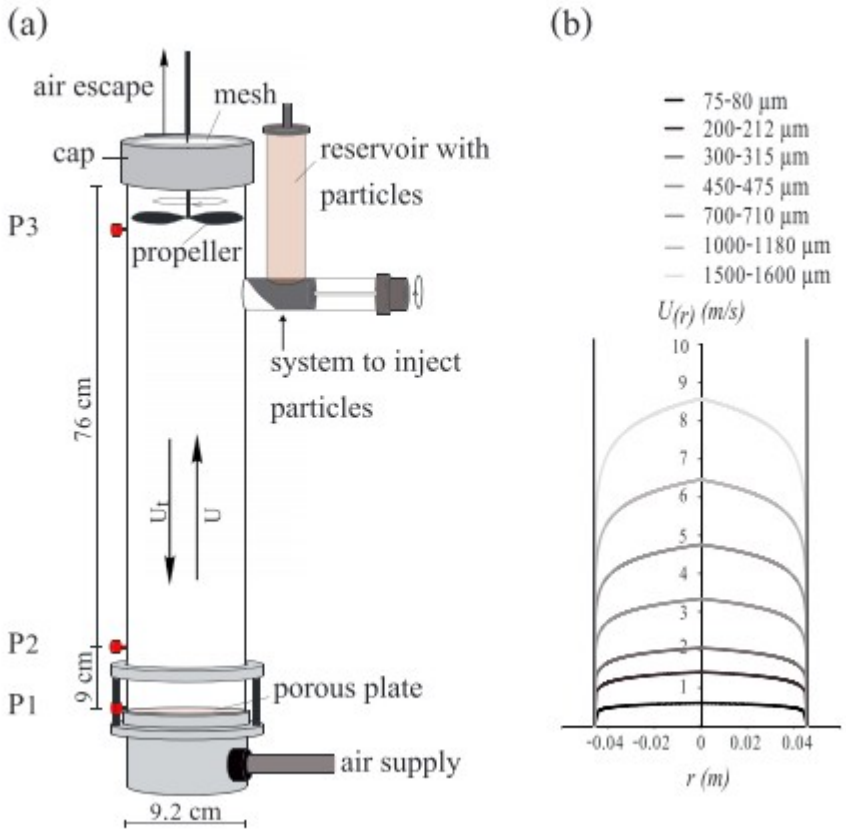

Figure 1

(a) Sketch of the experimental device consisting of a vertical perspex transparent cylinder, an air supply system from below, a system to inject the particles, pressure sensors (P) along the side of the cylinder, and a cap with a mesh and a propeller to keep the particles inside the pipe; the mean air flow velocity (U) is set equal to the settling velocity (U_t) of the particles. (b) Theoretical turbulent mean velocity profile for pure air flow for all investigated grain sizes (see supporting information).

and these smallest eddies have a typical time scale given by

$$\tau \sim Re^{-1/2} D/U. \qquad (3)$$

The addition of solid particles changes the bulk properties of the turbulent flow, so that the Reynolds number of the biphasic mixture is

$$Re_{mix} = \frac{\rho_{mix} UD}{\mu_{mix}}, \quad (4)$$

where ρ_{mix} and μ_{mix} are the density and the viscosity of the mixture, respectively, which are defined as

$$St_D = \tau_p \frac{U}{D}, \quad (7)$$

$$St_\tau = \frac{\tau_p}{\tau}. \quad (8)$$

with ρ_s and C as the density and the mean volume concentration of the particles, respectively (Einstein, 1906). Note that 6 is only a good approximation for low volume concentrations (<4 vol. % according to Brinkman, 1952), which is the case under consideration. Notice that calculations based on a more recent model by Mendoza and Santamaria-Holek (2009) show minor differences of less than 1% or 6% at volume fractions up to 4 vol. % or 10 vol. %, respectively.

The coupling of the particles to the turbulent eddies is characterized by the Stokes number for the largest (St_D) and the smallest eddies (St_τ), which is the ratio of the particle drag response time $\tau_p = (\rho_s - \rho)d^2/18\mu$ (with d as the diameter of the particle) to the overturn time of an eddy:

$$St_D = \tau_p \frac{U}{D}, \quad (7)$$

$$St_\tau = \frac{\tau_p}{\tau}. \quad (8)$$

Stokes numbers $\ll 1$ or $\gg 1$ indicate respectively efficient or poor coupling with the fluid (i.e., the particles act as good tracers of the fluid motion). Combining equations 4 and 7 shows that St_D is linked to the Reynolds number via the ratio $(d/D)^2$, so that

$$St_D \sim 10^{-4} Re_{mix} \quad (9)$$

for typical values of d and D considered in our study (see supporting information). Therefore, the Stokes numbers are always much larger than 1 in our experiments and both numbers cannot be investigated independently. As shown by Tsuji and Morikawa (1982) the presence of particles can also modify the velocity profile. For instance, particles of size of 200 μm change the shape of a turbulent flow velocity profile toward a laminar one, whereas larger particles (500–3,000 μm) can either widen the central plateau or cause the maximum velocity to migrate from the pipe axis toward the wall. Other studies in vertical risers have also investigated fluid velocities and particle motions in mixtures at different particle concentrations (Cao & Ahmadi, 1995; Lee & Durst, 1982; Qi et al., 2008; Shaffer et al., 2013; Tsuji & Morikawa, 1982).

A fundamental property of turbulent gas-particle flows is the presence of pervasive particle clusters that continuously form and break up (see the review of Fullmer & Hrenya, 2017). The clusters are aggregates of particles that have a higher bulk density and a smaller granular temperature (lower relative velocities between particles) than the surrounding flow. The relative gas-particle velocity is also smaller within the clusters than in the ambient mixture because the gas passes preferentially around the aggregates than through them. Clusters are characterized by a drag lower than that of individual particles in the more dilute surroundings. Cluster formation has two main origins. The first is the dissipation of the granular temperature, which causes a pressure gradient that drives particles from low to high concentration zones. The second is the hydrodynamic instabilities due to the relative motion between the solids and the gas, which lead to particle accumulation in form of waves that travel faster than the settling velocity of the individual particles. Nevertheless, the origins of cluster formation as a function of the Reynolds or the Stokes numbers, as reviewed in Fullmer and Hrenya (2017), are not yet well understood. Numerical simulations (Baker et al., 2017; Bec et al., 2007) suggested maximal clustering at $St_\tau \sim 1$ and a strong dependence of the particle concentration in clusters with the Stokes number but could not identify any clear trend of cluster formation as a function of St_τ or Re_{mix}. Chen et al. (2016) investigated, through numerical simulations and experiments, clustering in a vertical riser in which particles initially at rest at the bottom of the device were entrained upward by an air flow whose velocity was larger than the particles settling velocity. Their results revealed a heterogeneous solid fraction distribution, with maximum clustering at 10–15 vol. % mean concentration just above the initial bed of particles, and a more homogenous flow structure with particle concentrations down to 1–2 vol. % in upper parts of the riser. Similar experiments of Shaffer et al. (2013) revealed that the clusters were strongly sheared upward as the gas-particle mixture ascended into the riser.

3 Methodology

3.1 Experimental Device and Procedure

The experiments were performed at room temperature in a cylindrical pipe with dimensions of 85.2 cm in height and 9.2 cm in inner diameter (Figure 1). The pipe was connected to an air supply system at the base, which delivered mean air flow velocities of up to 7.5 m/s through a basal porous plate. It contained three sensors at different heights to measure the pressure of the air, as well as a system to inject particles incrementally at the top (Figure 1). The upper part of the pipe was closed with a cap consisting of a grid, which had different mesh sizes according to the different particle grain sizes used in the experiments. A propeller prevented possible accumulation of particles below the grid, and tests showed that it had a negligible influence on the results, including the pressure measurements. The experiments were observed with a Photron Fastcam SA3 high-speed video camera at 500–2,000 frames/s and with a maximum resolution of 1,024 × 1,024 pixels. The

recording time of single videos was between 10 and 30 s. The particles were nearly spherical glass beads of density ~2,500 kg/m^3 and of different grain size ranges according to the procedure we used (Table 1). Ideally, only one grain size for a given mixture should have been used, which was practically impossible. In consequence we sieved commercial batches of glass beads to narrow size ranges, which are given in Table 1. We used the average of the grain size range to calculate the values in Table 1, and the variation for each value within the particle size ranges was only ±6%.

Table 1
Particle Size Ranges and Corresponding Experimental Conditions

Particle size (μm)	75–80	200–212	300–315	450–475	700–710	1,000–1,180	1,500–1,600
Mesh size (μm)	100	250	450	630	800	1,700	1,700
Q (L/mn)	200	500	700	1,150	1,650	2,275	3,000
U (m/s)	0.5	1.3	1.8	2.9	4.1	5.8	7.5
U_t (m/s)	0.37	1.5	2.3	3.5	5.0	7.0	9.8
St_D	2.5×10^{-1}	4.5×10^{0}	1.4×10^{1}	5.3×10^{1}	1.7×10^{2}	5.7×10^{2}	1.5×10^{3}
St_τ	1.0×10^{1}	4.7×10^{2}	1.9×10^{3}	8.9×10^{3}	3.5×10^{4}	1.3×10^{5}	4.1×10^{5}
Re	3.1×10^{3}	7.7×10^{3}	1.1×10^{4}	1.8×10^{4}	2.5×10^{4}	3.5×10^{4}	4.6×10^{4}
Re_{mix}	8.9×10^{4}	2.5×10^{5}	4.3×10^{5}	6.2×10^{5}	9.8×10^{5}	1.8×10^{6}	2.5×10^{6}
Re_p	2.6×10^{0}	1.7×10^{1}	3.6×10^{1}	9.0×10^{1}	1.9×10^{2}	3.8×10^{2}	7.5×10^{2}
η (m)	2.2×10^{-4}	1.1×10^{-4}	8.7×10^{-5}	6.0×10^{-5}	4.6×10^{-5}	3.6×10^{-5}	2.9×10^{-5}
τ (s)	4.5×10^{-3}	7.0×10^{-4}	3.9×10^{-4}	1.9×10^{-4}	1.1×10^{-4}	7.2×10^{-5}	4.5×10^{-5}
C_{max} (average)	1.38	1.52	1.9	1.68	1.87	2.43	2.6
Number of experiments (measurements with pressure sensors)	7 (129)	3 (44)	4 (62)	4 (65)	3 (50)	3 (54)	3 (57)
Number of experiments (measurements with ball)	3 (32)	3 (36)	3 (45)	—	—	—	—

Note. Q and U = volume rate and mean velocity of the air flow; U_t = theoretical terminal fall velocity; St_D and St_τ = Stokes number of the largest or smallest eddies, respectively; Re and Re_{mix} = Reynolds number of the pure air flow or of the biphasic mixtures at maximum particle concentration (C_{max}) for the entire mixture above sensor P1; Re_p = particle Reynolds number; η and τ = Kolmogorov length and timescales; C_{max} = average of the maximum particle concentration for a number of experiments for each grain size range.

The principle of our experiments was that the air flow velocity was set to match the terminal settling velocity of the particles in order to obtain a quasi-static gas-particle mixture in the pipe in which the particle concentration could be measured accurately. Hence, we could investigate mixtures at different Reynolds numbers by varying the particle size. Reynolds numbers for the pure air flow above ~3,000 were chosen to ensure initial turbulent flow conditions. The Reynolds numbers of the mixtures were then calculated with equations 4–6, with C being the mean maximum particle concentration for each particle size range. With this approach we obtained maximum values of $Re_{mix} \sim 10^4$–10^6 (Table 1). Ideally, the particle size and the Stokes number should have been kept constant, while the Reynolds number was varied, which was impossible according to equation 9, and we acknowledge that this is a possible limitation of our experiments. We note, however, that the mean particle sizes were in a narrow range of the order of ~0.1–1 mm. The Stokes number for the largest and the smallest eddies in the system was considered and showed a range of values, which were in almost all cases much larger than 1 (Table 1), meaning poor coupling of the particles to the gas.

The theoretical settling velocity of the particles (U_t) was calculated according to the method of Rhodes (2008, pp. 29–33), which gave the particle Reynolds number

$$\mathrm{Re}_p = \frac{\rho U_t d}{\mu}, \qquad (10)$$

from the value of the drag coefficient in the intermediate turbulent regime at $\sim 1 < Re_p < 500$. In practice, values of U_t obtained this way appeared to be generally too high because with equivalent air flow velocities all the particles were entrained upward. In consequence, the mean air flow velocity needed to be turned down manually to obtain quasi-static mixtures (see Table 1). The velocity adjustment can be explained by the fact that the air flow velocity in the central part of the pipe was higher than the mean flow velocity owing to the shape of the velocity profile (Figure 1).

The particles were inserted stepwise in the device, from either the injection system at the top of the pipe while the air was flowing or they were poured first onto the basal porous plate before opening the air flow. Due to a higher accuracy, most of the experiments were performed using the second procedure, but both methods gave the same results. We employed bulk particle concentrations C (i.e., volume of particles divided by volume of the pipe) from 0.025 vol. % up to 8 vol. %, in steps of 0.1 vol. % (i.e., 14 ± 0.01 g). When the air flow velocity required to create a quasi-static mixture was reached, the pressure of the interstitial air was recorded by the sensors.

Different mesh sizes on the cap were used for the different particle sizes (Table 1). Preliminary tests with pure air flows showed that the grid did not generate any detectable additional dynamic pressure, meaning that the air escaped freely through it. With particles, however, meshes of the same size as that of the particles created an artificial overpressure. This might have been caused by accumulation of some particles in the interstices of the mesh, which might have prevented the air to leave the pipe freely. For this reason, we chose meshes with sizes slightly larger than the particle size. Larger mesh sizes prevented the accumulation of particles but allowed a small amount of particles to escape out of the pipe. The loss of particles was determined by weighing the material before and after the experiments, and conversion into volume showed that the loss was only of ~0.1 vol. % of the initial mass and hence had a negligible influence on the results.

3.2 Measurement of the Particle Concentration in the Dilute Mixtures

Preliminary tests showed that above a critical bulk particle concentration in the pipe, only a limited amount of particles could be suspended in the dilute mixture (which thus had a maximum concentration), while the other particles formed a basal dense fluidized bed. We used two methods to determine the solid volume concentrations in the dilute part.

We used piezoresistive sensors (Figure 1) to measure the pressure of the interstitial air in the mixtures, which was larger than the ambient atmospheric pressure due to the presence of the particles. The sensors were set in a casing whose extremity at the pipe inner wall was covered by a 36-

μm grid in order to measure the pressure of the interstitial air only. Notice that the sensors measured pressure differences relative to that of the atmosphere and that the dynamic component of the pressure equal to $\frac{1}{2}\rho_{air}U_{air}^2$ was negligible compared to the static component in almost all cases. The sensor at the bottom of the pipe (P1) measured the pressure related to all the particles, while the middle sensor (P2) was positioned 9 cm above the porous plate (and above any dense basal bed) in order to detect the pressure in the upper dilute mixture only. Tests showed that the motion of the propeller had a negligible influence on the measurements made with the top sensor (P3).

An empty plastic ball with a diameter of 3.88 cm, partly filled with glass particles (45–90 μm) to obtain a density (~1,000 kg/m^3) lower than the bulk density of the basal dense bed (~1,500 kg/m^3), was also used to probe the basal layer (Figure 2). The bulk density of a dense bed was estimated in experiments by the volume occupied by a known mass of particles. Before the air flow was turned on, either the ball was put on top of the porous plate before particles were added or the ball was gently put on top of a preexisting bed of particles resting on the porous plate. Hence, the ball moved either upward or downward according to its initial position once the air flow was turned on. The variation in ball height was determined from the variation of the length between the top of the ball and the top of the pipe, with an accuracy of ~0.5 mm. Below the critical bulk particle concentration, only a dilute gas-particle mixture formed and the ball ended in contact with the porous plate regardless of its initial position. Above the critical concentration, however, a fluidized bed could form and the ball adjusted its position by resting on top of it. The initial position of the ball did not influence the results.

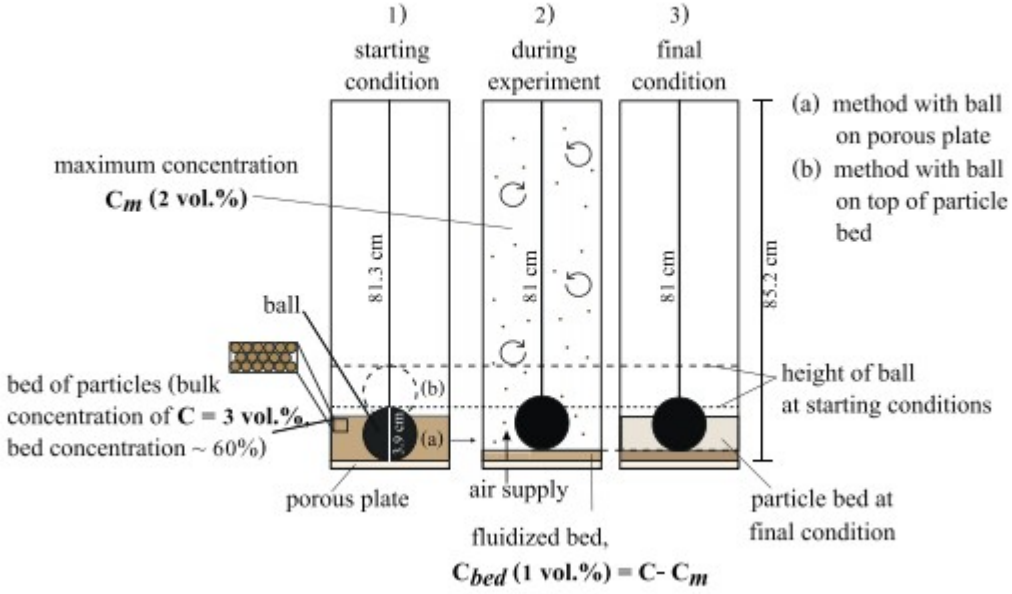

Figure 2

Illustration of the ball method in experiment with particle bulk concentration (C) larger than the critical concentration. The bulk concentration is defined as the ratio of the volume of the particles over the volume of the pipe. (1) Starting condition with the ball being either (a) in contact with the porous plate or (b) on top of a bed of particles. (2) The condition with air flow, with the upper dilute turbulent mixture at C_{max} and the basal dense fluidized bed at a concentration equal to C-C_{max}. (3) The final condition after the air flow is turned off, with the ball on top of the frozen particle bed and embedded within settled particles from the dilute suspension. Note that dimensions are not scaled.

4 Results

4.1 General Observations

For convenience we describe our experiments by referring to the particle size, but we recall that our aim was to investigate the mixtures as a function of the corresponding Reynolds numbers. For all particles sizes, the experiments showed the general trend of (i) a fully dilute suspension of particles at low concentrations in the pipe, which was smaller than a range of critical values C_{max} ~ 0.3–2.8 vol. %, and (ii) at bulk concentrations higher than C_{max}, particles separate into a basal dense fluidized bed and an upper dilute suspension with a particle concentration equal to C_{max} (Figure 3 and supporting information Movies S1–S5). The dilute suspensions at bulk concentrations below C_{max} were homogenous and showed no evidence of clusters. We observed homogeneous ascending motions in the pipe center and descending motions close to the wall, consistent with the air flow velocity profile. Clusters formed, however, at bulk concentrations larger than C_{max} at which the basal dense fluidized bed was created. At increasing Re_{mix} (with corresponding increasing particle size), the size of the clusters increased, whereas the number of the clusters decreased. Observations over a period of 1 s in three experiments revealed >10, 7–8, and 6 clusters for particle sizes of 75–80, 450–475, and 1,500–1,600 μm, respectively, and the size of the clusters increased from ~0.1–0.3 cm for the 75- to 80-μm particles to ~7 cm for the 450- to 475-μm particles. Overall, the clusters of smaller particles tended to coalesce and were sometimes indistinguishable from each other, whereas clusters of larger particles were more isolated and elongated in the vertical direction. The clusters also seemed to grow larger with increasing bulk particle concentration. For all particle sizes, the clusters showed preferentially wavelike downward motion along the walls or upward motion in the pipe center, like the surrounding dilute mixture, but some clusters clearly settled downward also in the central part of the pipe. In all cases, the relative motion of the clusters to the particles of the dilute mixture was oriented downward. The formation of a descending cluster is presented in Figure 4. Another important observation was that the settling clusters merged with the dense basal bed, from which particles seemed to be extracted either individually or in form of poorly defined aggregates that resembled the clusters but were significantly less concentrated. Because the clusters are transient and three-dimensional, quantifying their size, number, and longevity is challenging.

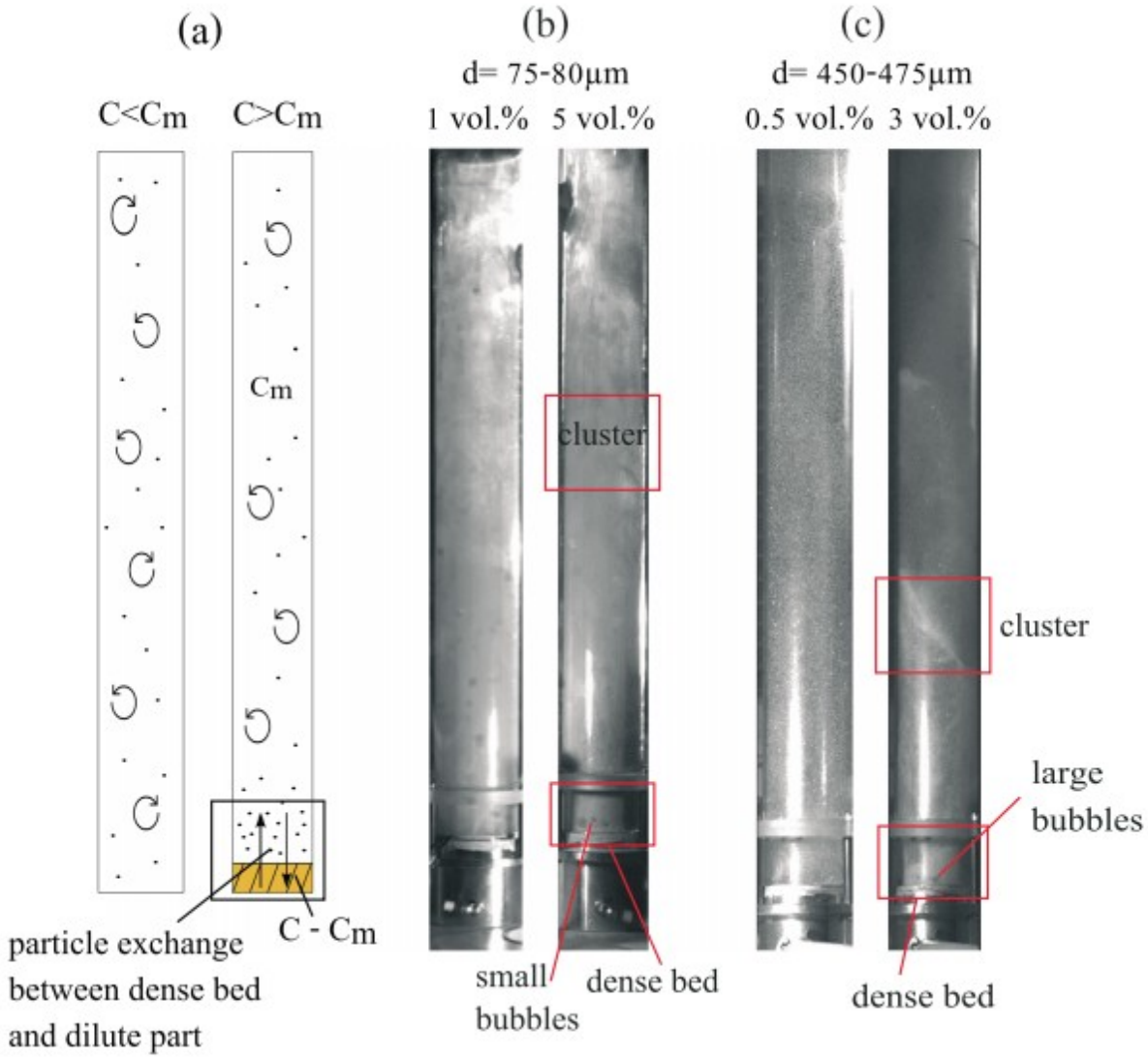

Figure 3

Structure of the mixtures showing a dilute suspension alone ($C < C_{max}$) or a dense basal fluidized bed and an upper dilute suspension ($C > C_{max}$) at bulk concentrations below or above the critical concentration, respectively. (a) Sketch of the two conditions including particle exchange between the bed and the dilute part at $C > C_{max}$; (b) 75- to 80-μm particles ($Re_{mix} = 8.9 \times 10^4$) at 1 or 5 vol. %; (c) 450- to 475-μm particles ($Re_{mix} = 6.1 \times 10^5$) at 0.5 or 3 vol. %.

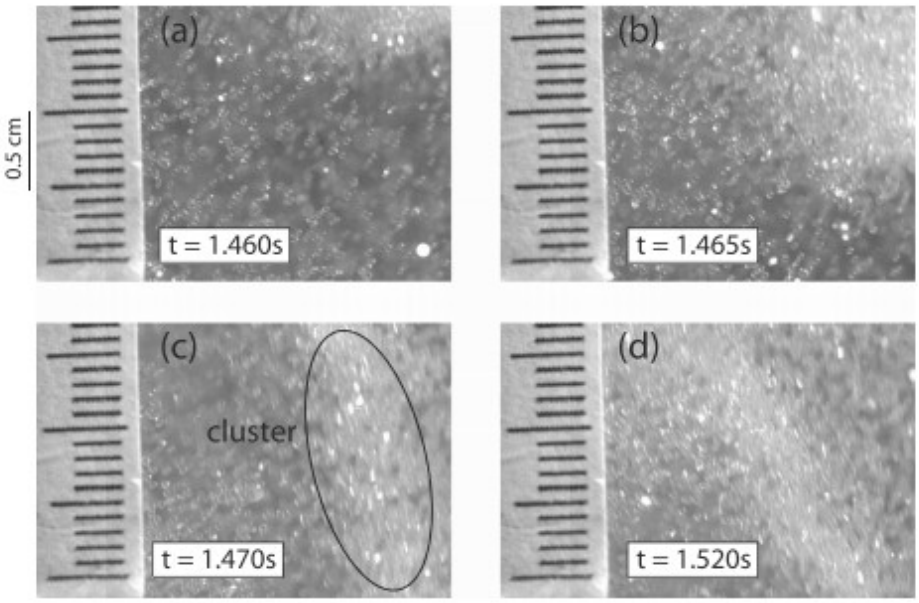

Figure 4

Cluster formation in a mixture of 450- to 475-μm particles filmed at 2,000 frames/s. Snapshots in (a) to (d) show the downward motion of the cluster at the wall. Descending clusters were also observed at the pipe center and for other particle sizes.

The basal dense fluidized bed contained air bubbles whose size increased with increasing bed thickness and particle size. The air flow velocity being 2 orders of magnitude larger than the minimum fluidization and bubbling velocities, the beds were characterized by the bubbling and spouting regimes typical of the Geldart classification. Hence, beds of particles of 300–315 μm and smaller had bubbles whose size grew with the air flow velocity, whereas beds of larger particles were characterized by a vigorous spouting regime and in consequence had a poorly defined upper surface.

The transition between the dense and the dilute parts was rather sharp for large particle sizes but showed a concentration gradient with a decrease in particle concentration toward the upper dilute suspension as the particle size decreased. In the latter case, the particles were more concentrated in a narrow zone between the top of the bed and approximately the level of the pressure sensor P2, and the less concentrated mixture above the sensor was homogeneous. The rate of particle exchange between the dense bed and the dilute part seemed to increase with the particle size as the cluster size increased, though the clusters were less numerous and formed less frequently.

4.2 Particle Concentration in the Dilute Mixtures

The basal sensor (P1) detected air pressure larger than that of the ambient atmosphere at all bulk concentrations, which were as low as 0.025 vol. % (Figure 5). The pressure increased with increasing concentration, and it was, in fact, equal to the weight of the particles divided by the cross-sectional

area of the pipe, demonstrating that this weight was entirely supported by the drag force generated by the air flow and that the corresponding pressure was transmitted to the sensor through the interstitial air (Figure 5). The pressure measured by the top sensor (P3) was almost equal to the atmospheric pressure, suggesting a negligible amount of particles between the sensor and the cap. The sensor just above the dense bed (P2) showed an increase in pressure up to the critical bulk particle concentration. Above this critical concentration pressure was nearly constant in all cases, except for the smallest particles of 75–80 µm, hence suggesting that a maximum particle concentration in the dilute upper mixture was reached (Figure 6).

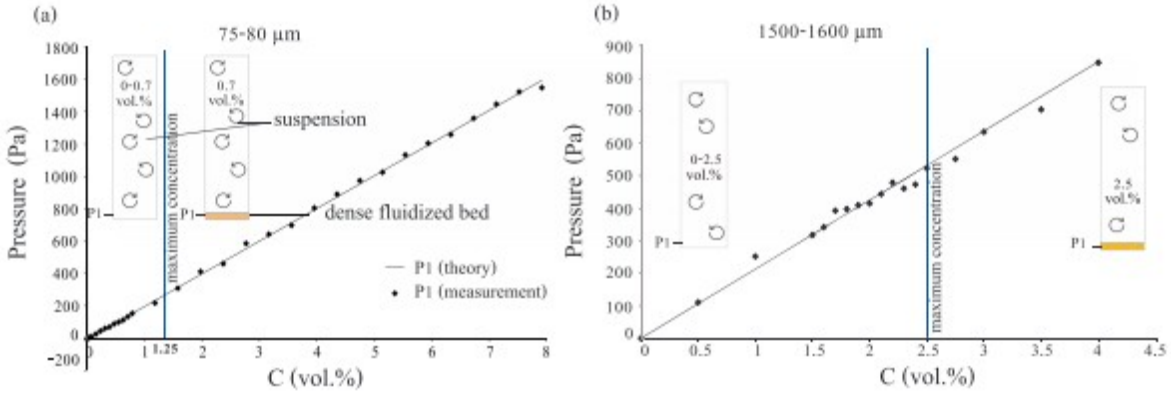

Figure 5

Air pressure as a function of the bulk particle concentration, measured with sensor P1 for (a) 75- to 80-µm particles with maximum $Re_{mix} = 8.9 \times 10^4$, and (b) 1,500- to 1,600-µm particles with maximum $Re_{mix} = 2.5 \times 10^6$. Pressure measurements match almost perfectly with the theoretical pressure equal to the weight of the particles over the cross-sectional area of the pipe. Maximum concentration refers to the dilute mixture.

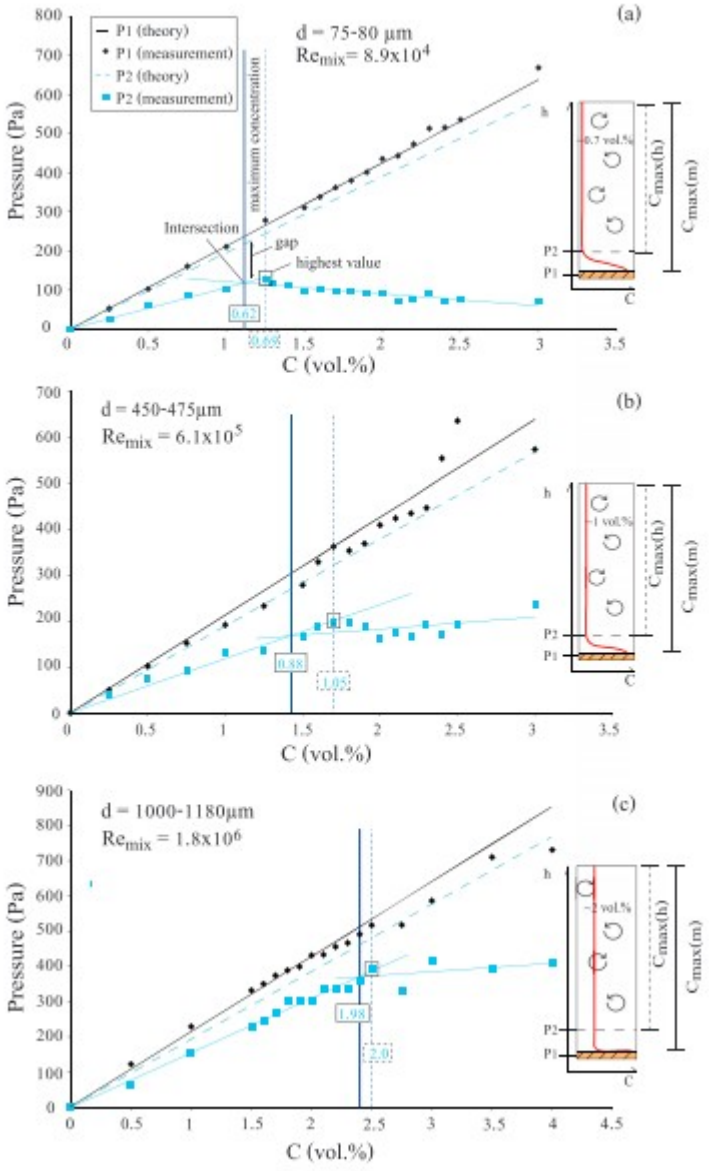

Figure 6

Air pressure measured with sensors P1 and P2 as a function of the bulk particle concentration for three different mixtures (see particle sizes and mixture Reynolds numbers at maximum concentration in the dilute part). The theoretical pressure is given by the weight of the particles above the sensor (assuming homogeneous mixture above P2) divided by the cross-sectional area of the pipe. The dark blue lines indicate the mean maximum particles concentrations of the dilute mixtures (below and above P2), from which maximum particle concentrations in the homogeneous part (above P2) are calculated (values in rectangles). The red lines in the sketches indicate the possible particle concentration in the pipe.

Notice that the pressure measured at a given bulk concentration was in all cases stable over durations of at least ~20 s. Due to the stability of the pressure signal and the small background noise of the sensors (±5 to 10 Pa), an average value of 100–200 pressure data was chosen as the mean pressure value for each particle concentration.

The maximum particle concentration in the dilute mixtures was determined according to the following procedure. We first retrieved the maximum mean concentration for the entire dilute mixtures ($C_{max(m)}$), that is, above and below the sensor P2, from either the intersection of the two pressure curves obtained with P2 or the highest pressure value close to the transition at C_{max}. Both methods gave very similar results (Figure 6). The values of $C_{max(m)}$are presented in Figure 7 as a function of Re_{mix}. $C_{max(m)}$ increases from ~1 to 2.8 vol. % for Re_{mix} of ~10^4 to ~10^6, and it scales with ~$Re_{mix}^{1/5}$ (values are given in the supporting information). At this maximum mean concentration, however, the pressure measured by the sensor P2 was less than the theoretical value assuming a homogeneous mixture and full support of the weight of the particles present above the sensor (Figure 6). This gap in pressure suggested that the particle concentration in the dilute mixture was not homogeneous and was higher below the sensor P2 than above it. Consequently, we calculated the particle concentration in the homogeneous dilute part above the sensor by taking into account this difference in pressure. The gap, however, decreased notably as the particle size and the corresponding mixture Reynolds number increased, hence suggesting more homogeneous mixtures. The maximum particle concentration of the homogeneous dilute mixtures ($C_{max(h)}$) above the sensor P2 determined this way is shown in Figure 7. It increases from ~0.3 to 2.8 vol. % for Re_{mix} of ~10^4 to ~10^6, and it scales approximately with ~$Re_{mix}^{1/2}$ (values are given in the supporting information). The values of $C_{max(h)}$ for the 75- to 80-µm particles were somewhat higher than for the 200- to 212-µm and 300- to 315-µm particles. They fell slightly off the trend of the other particle sizes and were therefore not considered for determining the correlation with Re_{mix}.

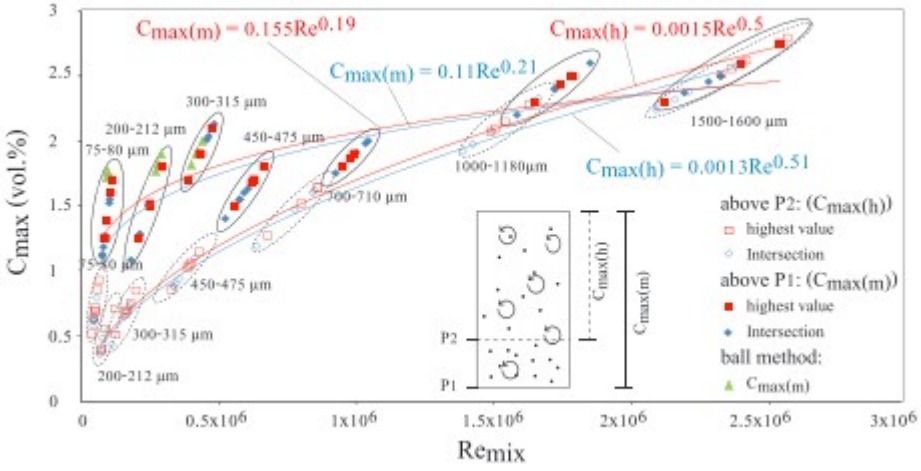

Figure 7

Maximum particle concentration in the dilute mixtures (C_{max}) as a function of the mixture Reynolds number (Re_{mix}). Note that error bars are smaller than the symbols. Mean particle concentrations ($C_{max(m)}$) from the ball method (filled green symbols) and the pressure sensors show a good agreement for the three smallest particle sizes. The particle concentrations in the homogeneous part ($C_{max(h)}$) above the pressure sensor P2, marked with empty symbols, are also shown for all investigated particle

sizes. The drawn oval circles group all measurements for a given particle size. The data indicate an increase of $C_{max(h)}$ with $Re_{mix}^{1/2}$and of $C_{max(m)}$ with $Re_{mix}^{1/5}$.

The ball method yielded results only for the three smallest particle sizes (75–80, 200–212, and 300–315 μm). The experiments were repeated at least three times per particle size and showed similar results for a given mixture (Figure 7 and supporting information). Due to spouting processes, particles of size 450–475 and larger could not be investigated because the ball could not rest on top of the beds. It is important to note that the ball method only provided mean values of the maximum concentration in the dilute (cf. $C_{max(m)}$) part. For the three grain sizes investigated, the mean maximum concentration increased slightly with increasing particle size. The values were close to those obtained with the pressure sensors, suggesting that the ball had a negligible effect on the turbulent air flow and on the structure of the mixture in the pipe.

5 Discussion

The dilute turbulent gas-particle mixtures in our experiments always had maximum particle concentrations C_{max} lower than ~2.8 vol. %. We now discuss the origin of this maximum concentration, its consequences for the structure of the mixtures in the experiments, and its implications for geophysical systems.

5.1 Maximum Particle Concentration in Dilute Mixtures

Our experiments revealed that the occurrence of a maximum particle concentration in the dilute mixtures coincided with the emergence of clusters. This suggests that the dissipation of the granular temperature and the hydrodynamic instabilities were high enough to promote the formation of clusters (Fullmer & Hrenya, 2017) once this critical concentration was reached, and that clustering enhanced settling and hence prevented higher concentrations. The clusters had a settling velocity higher than that of the individual particles owing to their lower drag, and in consequence they decoupled from the bulk mixture and moved downward. The consequence of clustering at bulk concentrations $C > C_{max}$ was the development of a bimodal structure in the pipe, which consisted of a basal dense fluidized bed and an overlying dilute mixture at concentration equal to C_{max}. The dilute mixtures had several remarkable properties, which we discuss below.

The particle concentration of the dilute mixtures above the dense beds was constant over time at given bulk concentration, which suggests that there was a continuous mean mass balance between clusters decoupling from the dilute mixture and feeding the bed and particles leaving the bed and injected into the dilute part. It is likely that extraction of particles from the bed occurred in the central region where the air flow velocity was slightly larger than the particle settling velocity. These particles locally increased the particle concentration of the dilute suspension until conditions for clustering were met. The new clusters settled and merged with the bed, and as a consequence the mean concentration in the dilute mixture decreased slightly

below the maximum concentration. Particles thus cycled between the dilute and concentrated regions.

The dilute mixtures had a more concentrated lower part, between the dense bed and approximately the level of the pressure sensor P2, but they became more homogenous as the particle size, Re_{mix} and St_D (and St_τ), and the cluster size increased, and as the number and frequency of the clusters decreased. Determining which of these parameters controlled the development of more homogenous mixtures is not straightforward since they could not be varied independently, a limitation of our experiments owing to the fixed tube diameter and the dependence of St_D on Re_{mix} (see equation 9). However, the general trend suggests that more homogenous concentrations could have been favored by (i) higher turbulence at larger Re_{mix} but also because of coarser particle sizes (Fessler et al., 1994; Tsuji & Morikawa, 1982), (ii) less efficient air-particle coupling (i.e., larger Stokes numbers), and/or (iii) settling of a decreasing number of less frequent but larger clusters. In this context, we stress that the mixtures of the smallest particles of 75–80 µm had Reynolds numbers indicating a flow regime close to the laminar-turbulent transition, which might explain their more pronounced concentration gradient, mainly at $C > C_{max}$ when the dense bed was present (Figure 6), and why their maximum concentrations in the homogeneous part were off the trend defined by the other mixtures (Figure 7).

Another important property of the dilute mixtures was that their maximum particle concentration increased with either $Re_{mix}^{1/5}$ or $Re_{mix}^{1/2}$, considering respectively the whole dilute mixture or only its homogenous upper part. Notice that clustering could also be favored by low Stokes numbers (Bec et al., 2007; Qi et al., 2008), which could explain the lower values of C_{max} for the mixtures at lower Re_{mix} containing particles of smaller size.

Finally, the air pressure in the dilute mixtures showed that the weight of the particles was counterbalanced by the fluid drag at concentrations down to 0.025 vol. %, and in this regard it was similar to the interstitial pore fluid pressure of dense fluidized beds (Rhodes, 2008). The interstitial air pressure was still transmitted to the sensor even though the gaps between the particles were several orders of magnitude larger than the pores in compacted granular beds.

5.2 Implications for Natural Systems

We now discuss the implications of our results for geophysical gas-particle mixtures, focusing on volcanic events, and highlight the main limitations and how the experimental data may be extrapolated. We consider the particle concentration in dilute mixtures essentially as a function of the Reynolds number because a typical value of this parameter can be estimated for most geophysical flows.

A first important limitation of our experiments is the range of Reynolds numbers we investigated, which was up to $Re_{mix} \sim 10^6$, while natural geophysical mixtures may have Reynolds numbers up to ~10^9–10^{10} (e.g., Andrews & Manga, 2012). Another limitation is the investigation of spherical particles with only one grain size and Stokes numbers larger than ≈1, whereas natural mixtures commonly contain particles of various grain sizes and shapes and with wider ranges of Stokes numbers (Burgisser et al., 2005; Jessop et al., 2016).

A key feature of our experiments is the formation of clusters, which are fundamentally transient structures (Fullmer & Hrenya, 2017). Clusters form when a dense granular medium, possibly at solid concentrations up to ~50–60 vol. %, evolves to a dilute mixture having concentrations of the order of 1 vol. %, and clusters at intermediate concentrations can exist only for limited periods of time and over limited length scales (Chen et al., 2016). Clusters also form when a dilute suspension deflates to form a dense granular medium (Breard et al., 2017, 2016; Lube et al., 2015). This suggests that the range of solid concentrations that can be stable over long time and length scales in geophysical gas-particle flows may be bimodal, with end-members represented by highly concentrated (fluidized) mixtures and dilute turbulent mixtures.

Our experiments provide insights into the possible maximum particle concentration in dilute natural mixtures and how this concentration may vary with the Reynolds number. We observed that the maximum concentration in our experimental flows scaled with $Re_{mix}^{1/5}$when considering the entire dilute mixtures. Assuming that the same law applies, maximum particle concentrations scaling with $Re_{mix}^{1/5}$ would be up to ~8–14 vol. % at Re_{mix} of 10^9–10^{10}. However, we question whether the same scaling law may strictly apply for natural systems at $Re_{mix} > 10^6$. First, mixtures with concentrations of ~8–14 vol. % could be dominated by particle-particle interactions and would not behave as in experiments. Second, the natural systems at high Reynolds numbers could be characterized by physical regimes different than in experiments at lower Reynolds number. Third, the one-fifth power law depends on the results of the experiments at the lowest Re_{mix} and which lie in the transitional regime rather than in the fully turbulent regime; hence, the maximum particle concentrations in natural systems at high Re_{mix} could actually be close to the highest values of 2.5–3 vol. % found in experiments in the fully turbulent regime and which define a plateau. Another way to extrapolate the empirical results to natural systems is to consider the processes at the particle scale and hence the Reynolds number of the particles in the mixtures (Re_p). In this context, the particles that could be suspended in the dilute part of flows at Re_{mix} of 10^9–10^{10}(at vertical velocities of ~50–100 m/s) would have a maximum size of the order of 1–10 cm and particle Reynolds numbers of 15×10^3–500×10^3. Considering that the maximum particle concentration scales with $Re_p^{0.11}$ (see supporting

information), then C_{max} for these particles would be 3.1 vol. % (1 cm) and 4.7 vol. % (10 cm), with settling velocities of 25 and 78 m/s, respectively.

The particle concentration in volcanic mixtures generated by explosive eruptions can be evaluated in light of our results and of the literature on gas-particle systems. These eruptions are characterized by three stages during which biphasic mixtures may evolve from dense to dilute and vice versa, that is, a conduit flow, followed by the generation of a plume, which may collapse to form pyroclastic density currents. The vertical setup of our experiments is more relevant to conduit flows and plumes and also allows us to address vertical turbulent fluid flow motions in pyroclastic density currents although the overall direction in these flows is horizontal rather than vertical. Nevertheless, since clusters tend to elongate parallel to the vorticity vector (Baker et al., 2017), which is horizontal in both our experiments and propagating density currents, the structure of clusters may be similar.

Shock tube experiments provide complementary insights. Anilkumar et al. (1993) and Cagnoli et al. (2002) reported that experiments simulating conduit flow the ascending gas-particle mixture had regions of high particle concentrations surrounded by more dilute parts. They argued that mixtures ejected at volcanic vents could be highly heterogeneous. The concentrated regions they observed were probably clusters, which formed as an initial dense granular bed expanded upward as a consequence of rapid internal gas decompression. Experiments in large risers (cf. Chen et al., 2016), however, show that in a similar configuration the clusters dilate and disappear progressively, while they move upward, hence leading to dilute turbulent mixtures at solid concentrations of ≈1 vol. %. This suggests that mixtures ejected at volcanic vents may be homogeneous and with very low particle load, in agreement with models (Dufek & Bergantz, 2007; Esposti Ongaro et al., 2002, 2011; Neri et al., 2014).

Clusters could arise in volcanic plumes and in pyroclastic density currents in regions where the local particle concentration would increase to attain a critical value, as shown by our experiments. Clusters might contribute to generate the finger-like gravitational instabilities at the base of umbrella clouds (Carazzo & Jellinek, 2012; Manzella et al., 2015), but more likely they would form following the collapse of an unstable plume as particles rapidly and progressively accumulate above the ground, which results in a particle concentration increase and generates pyroclastic density currents (Breard et al., 2017; Sweeney & Valentine, 2017; Valentine & Sweeney, 2018). Settling of clusters in the emerging current may then contribute to further increase the mixture concentration downward, as demonstrated in the experiments of Breard et al. (2016). In these experiments, clusters settle down from an upper turbulent suspension with particle concentrations lower than ~1–2 vol. % and they accumulate to feed a basal highly concentrated avalanche. Notice that the maximum particle concentrations of dilute mixtures measured in our experiments closely match with the concentrations observed in this upper suspension at similar Reynolds numbers. Clustering

might also control the depositional processes of pyroclastic density currents whose deposits may contain lenses or pockets of large clasts, which might have settled rapidly through clusters. A scaling issue arises when considering the relative thickness of such a transitional zone of clusters in pyroclastic density currents (and possibly in snow avalanches), and we argue that there are two possibilities. If the thickness of the cluster zone scales with the characteristic length scale of the system, and hence with the flow velocity and the Reynolds number, then it will represent a significant portion of the whole current thickness. If, in contrast, it scales with the particle size, then it will have a negligible relative thickness and the current will consist fundamentally of a dense gas-particle flow overridden by a dilute turbulent cloud. Our experiments also provide constraints on the particle concentrations of ash clouds generated through ash venting in ash-filled cracks formed during lava dome emplacement (Black et al., 2016).

6 Conclusions

We investigated the solid phase concentration in geophysical dilute turbulent gas-particles mixtures through laboratory experiments in a vertical pipe. The experimental mixtures had Reynolds numbers $Re_{mix} \sim 10^4$–10^6 and contained particles of sizes of ~0.1–1 mm and Stokes numbers >~1. The main conclusions of our study are the following.

1. The dilute mixtures had maximum concentrations of ~0.3–2.8 vol. % set by the formation of clusters and which scaled with either $Re_{mix}^{1/5}$, when considering the entire dilute mixtures, or $Re_{mix}^{1/2}$, when considering only the upper homogeneous part of the mixtures. The scaling with $Re_{mix}^{1/5}$ for the whole dilute mixture is probably more relevant to natural systems. Though the particles were poorly coupled to the turbulent gas (i.e., $St > 1$) in almost all cases, these scaling laws might also depend on the Stokes number.
2. The clusters decoupled from the surrounding mixture and settled to form a basal dense fluidized bed. Constant particle concentration of the dilute mixtures over time suggested a mean mass balance between the clusters feeding the bed and particles ejected from the bed into the upper dilute part.
3. Air pressure indicating full support of the weight of the particles by the gas flow drag, similar to the interstitial pore fluid pressure in highly concentrated biphasic mixtures, was measured at particle concentrations down to 0.025 vol. %. This shows that particle concentration can be retrieved from fluid pressure measurements even in very dilute mixtures.
4. Geophysical gas-particle mixtures with Reynolds numbers lower than $\sim 10^6$ may have maximum solid concentrations similar to those determined experimentally. An uncertainty remains concerning the applicability of the empirical scaling laws we found to natural systems at higher Reynolds numbers, and this issue requires further investigation.

The experiments in the fully turbulent regime, however, point toward possible maximum concentrations of approximately a few volume percent when considering likely values of the mixture or the particle Reynolds numbers in nature.

5. The maximum particle concentrations in dilute mixtures that can be inferred from our experiments may provide constraints on the input and output parameters of models aimed to simulate turbulent gas-particle flows and on the data retrieved from geophysical observations.

6. Owing to the transient nature of clusters, which form when a dilute suspension transforms into a dense granular medium or vice versa, the range of solid concentrations in geophysical systems could be essentially bimodal and characterized by granular mixtures at nearly maximum particle concentration and turbulent suspensions with concentrations less than ≈1 vol. %. These two end-members may coexist in many natural gravitational flows like snow avalanches and pyroclastic density currents. Particles may move repeatedly between the dense and dilute region.

Notation

C	bulk particle concentration in the pipe.
C_{max}	maximum particle concentration.
$C_{max(m)}$	mean maximum particle concentration of the dilute part.
$C_{max(h)}$	maximum particle concentration in homogeneous dilute part.
d	particle diameter.
D	pipe diameter.
Q	air flow rate.
Re	Reynolds number of the particle-free flow.
Re_{mix}	Reynolds number of the gas-particle mixture.
Re_p	particle Reynolds number (particle in a pure fluid).
St_D	Stokes number for largest eddies.
St_τ	Stokes number for smallest eddies.
U_t	terminal particle settling velocity.
U	mean velocity of particle-free flow.
μ	fluid (air) dynamic viscosity.
μ_{mix}	viscosity of the gas-particle mixture.
ρ	density of the fluid (air).
ρ_s	density of the solid particles.
ρ_{mix}	density of the gas-particle mixture.
η	Kolmogorov length scale.
τ	Kolmogorov time scale.

Acknowledgments

This research was financed by the French Government Laboratory of Excellence initiative ANR-10-LABX-0006 through a doctoral scholarship (A. Weit), by the French National Research Agency (ANR) RAVEX project, and by the French Research Institute for sustainable Development (IRD). This is

Laboratory of Excellence ClerVolc contribution 298. M. M. is supported by NSF 1447559. We thank Gert Lube and Eric Breard for useful discussion on cluster formation, Cyrille Guillot for constructing the device and his valuable technical expertise, and Ben Andrews and an anonymous reviewer for insightful reviews. The data used are listed in the references, tables, and supporting information.

References

Andrews, B. J., & Manga, M. (2012). Experimental study of turbulence, sedimentation, and coignimbrite mass partitioning in dilute pyroclastic density currents. *Journal of Volcanology and Geothermal Research*, 225-226, 30– 44. https://doi.org/10.1016/j.jvolgeores.2012.02.011

Anilkumar, A. V., Sparks, R. S. J., & Sturtevant, B. (1993). Geological implications and applications of high-velocity two-phase flow experiments. *Journal of Volcanology and Geothermal Research*, 56(1–2), 145– 160. https://doi.org/10.1016/0377-0273(93)90056-W

Baker, L., Frankel, A., Mani, A., & Coletti, F. (2017). Coherent clusters of inertial particles in homogeneous turbulence. *Journal of Fluid Mechanics*, 833, 364– 398. https://doi.org/10.1017/jfm.2017.700

Bec, J., Biferale, L., Cencini, M., Lanotte, A., Musacchio, S., & Toschi, F. (2007). Heavy particle concentration in turbulence at dissipative and inertial scales. *Physical Review Letters*, 98(8), 1– 4. https://doi.org/10.1103/PhysRevLett.98.084502

Black, B. A., Manga, M., & Andrews, B. (2016). Ash production and dispersal from sustained low-intensity Mono-Inyo eruptions. *Bulletin of Volcanology*, 78(8), 57– 70. https://doi.org/10.1007/s00445-016-1053-0

Breard, E. C. P., Dufek, J., & Lube, G. (2017). Enhanced mobility in concentrated pyroclastic density currents: An examination of a self-fluidization mechanism. *Geophysical Research Letters*, 45, 654– 664. https://doi.org/10.1002/2017GL075759

Breard, E. C. P., Lube, G., Jones, J. R., Dufek, J., Cronin, S. J., Valentine, G. A., & Moebis, A. (2016). Coupling of turbulent and non-turbulent flow regimes within pyroclastic density currents. *Nature Geoscience*, 9(10), 767– 771. https://doi.org/10.1038/ngeo2794

Brinkman, H. C. (1952). The viscosity of concentrated suspensions and solutions. *The Journal of Chemical Physics*, 20(4), 571. https://doi.org/10.1063/1.1700493

Burgisser, A., Bergantz, G. W., & Breidenthal, R. E. (2005). Addressing complexity in laboratory experiments: The scaling of dilute multiphase flows in magmatic systems. *Journal of Volcanology and Geothermal Research*, 141(3–4), 245– 265. https://doi.org/10.1016/j.jvolgeores.2004.11.001

Cagnoli, B., Barmin, A., Melnik, O., & Sparks, R. S. J. (2002). Depressurization of fine powders in a shock tube and dynamics of fragmented magma in volcanic conduits. *Earth and Planetary Science Letters*, 204(1-2), 101– 113. https://doi.org/10.1016/S0012-821X(02)00952-4

Cantero, M. I., Cantelli, A., Pirmez, C., Balachandar, S., Mohrig, D., Hickson, T. A., & Parker, G. (2012). Emplacement of massive turbidites linked to extinction of turbulence in turbidity currents. *Nature Geoscience*, 5(1), 42– 45. https://doi.org/10.1038/ngeo1320

Cantero, M. I., Shringarpure, M., & Balachandar, S. (2012). Towards a universal criteria for turbulence suppression in dilute turbidity currents with non-cohesive sediments. *Geophysical Research Letters*, 39, L14603. https://doi.org/10.1029/2012GL052514

Cao, J., & Ahmadi, G. (1995). Gas-particle two-phase turbulent flow in a vertical duct. *International Journal of Multiphase Flow*, 21(6), 1203– 1228. https://doi.org/10.1016/0301-9322(95)00042-V

Carazzo, G., & Jellinek, M. A. (2012). A new view of the dynamics, stability and longevity of volcanic clouds. *Earth and Planetary Science Letters*, 325-326, 39– 51. https://doi.org/10.1016/j.epsl.2012.01.025

Carazzo, G., Kaminski, E., & Tait, S. (2008). On the dynamics of volcanic columns: A comparison of field data with a new model of negatively buoyant jets. *Journal of Volcanology and Geothermal Research*, 178(1), 94– 103. https://doi.org/10.1016/j.jvolgeores.2008.01.002

Chen, C., Dai, Q., & Qi, H. (2016). Improvement of EMMS drag model for heterogeneous gas-solid flows based on cluster modeling. *Chemical Engineering Science*, 141, 8– 16. https://doi.org/10.1016/j.ces.2015.10.025

Davidson, P. A. (2015). *Turbulence: An introduction for scientists and engineers* (2nd ed.). New York: Oxford University Press. https://doi.org/10.1093/acprof:oso/9780198722588.001.0001

Del Bello, E., Taddeucci, J., de' Michieli Vitturi, M., Scarlato, P., Andronico, D., Scollo, S., et al. (2017). Effect of particle volume fraction on the settling velocity of volcanic ash particles: Insights from joint experimental and numerical simulations. *Scientific Reports*, 7, 39620. https://doi.org/10.1038/srep39620

Dufek, J. (2016). The fluid mechanics of pyroclastic density currents. *Annual Review of Fluid Mechanics*, 48(1), 459– 485. https://doi.org/10.1146/annurev-fluid-122414-034252

Dufek, J., & Bergantz, G. W. (2007). Suspended load and bed-load transport of particle-laden gravity currents: The role of particle-bed interaction. *Theoretical and Computational Fluid Dynamics*, 21(2), 119– 145. https://doi.org/10.1007/s00162-007-0041-6

Einstein, A. (1906). Eine neue Bestimmung der Moleküldimensionen. *Annalen der Physik*, 324(2), 289– 306. https://doi.org/10.1002/andp.19063240204

Esposti Ongaro, T., Neri, A., Todesco, M., & Macedonio, G. (2002). Pyroclastic flow hazard assessment at Vesuvius (Italy) by using numerical modeling. II. Analysis of flow variables. *Bulletin of Volcanology*, 64(3–4), 178– 191. https://doi.org/10.1007/s00445-001-0190-1

Esposti Ongaro, T., Widiwijayanti, C., Clarke, A. B., Voight, B., & Neri, A. (2011). Multiphase-flow numerical modeling of the 18 May 1980 lateral blast at Mount St. Helens, USA. *Geology*, 39(6), 535– 538. https://doi.org/10.1130/G31865.1

Fessler, J. R., Kulick, J. D., & Eaton, J. K. (1994). Preferential concentration of heavy particles in a turbulent channel flow. *Physics of Fluids*, 6(11), 3742– 3749. https://doi.org/10.1063/1.868445

Fullmer, W. D., & Hrenya, C. M. (2017). The clustering instability in rapid granular and gas-solid flows. *Annual Review of Fluid Mechanics*, 49(1), 485– 51010.1146/annurev-fluid-010816-060028

Goudie, A. S., & Middleton, N. J. (2001). Saharan dust storms: Nature and consequences. *Earth-Science Reviews*, 56(1–4), 179– 204. https://doi.org/10.1016/S0012-8252(01)00067-8

Jessop, D. E., Gilchrist, J., Jellinek, A. M., & Roche, O. (2016). Are eruptions from linear fissures and caldera ring dykes more likely to produce pyroclastic flows? *Earth and Planetary Science Letters*, 454, 142– 153. https://doi.org/10.1016/j.epsl.2016.09.005

Köhler, A., McElwaine, J. N., Sovilla, B., Ash, M., & Brennan, P. (2016). The dynamics of surges in the 3 February 2015 avalanches in Vallée de la Sionne. *Journal of Geophysical Research: Earth Surface*, 121, 2192– 2210. https://doi.org/10.1002/2016JF003887

Lee, S. L., & Durst, F. (1982). On the motion of particles in turbulent duct flows. *International Journal of Multiphase Flow*, 8(2), 125– 146. https://doi.org/10.1016/0301-9322(82)90013-1

Louge, M. Y., Carroll, C. S., & Turnbull, B. (2011). Role of pore pressure gradients in sustaining frontal particle entrainment in eruption currents: The case of powder snow avalanches. *Journal of Geophysical Research*, 116, F04030. https://doi.org/10.1029/2011JF002065

Lube, G., Breard, E. C. P., Cronin, S. J., & Jones, J. (2015). Synthesizing large-scale pyroclastic flows: Experimental design, scaling, and first results from PELE. *Journal of Geophysical Research: Solid Earth*, 120, 1487– 1502. https://doi.org/10.1002/2014JB011666

Manzella, I., Bonadonna, C., Phillips, J. C., & Monnard, H. (2015). The role of gravitational instabilities in deposition of volcanic ash. *Geology*, 43(3), 211– 214. https://doi.org/10.1130/G36252.1

Mendoza, C. I., & Santamaria-Holek, I. (2009). The rheology of hard sphere suspensions at arbitrary volume fractions: An improved differential viscosity model. *Journal of Chemical Physics*, 130(4), 044904. https://doi.org/10.1063/1.3063120

Neri, A., Esposti Ongaro, T., Voight, B., & Widiwijayanti, C. (2014). Pyroclastic density current hazards and risk. In J. F. Shroder & P. Papale (Eds.), *Volcanic hazards, risks and disasters* (pp. 109– 140). Amsterdam, Netherlands: Elsevier. https://doi.org/10.1016/B978-0-12-396453-3.00005-8

Qi, X. B., Zhang, H., & Zhu, J. (2008). Solids concentration in the fully developed region of circulating fluidized bed downers. *Powder Technology*, 183(3), 417– 425. https://doi.org/10.1016/j.powtec.2008.01.018

Rhodes, M. (2008). *Introduction to particle technology: Second edition*. West Sussex, England: John Wiley and Sons Ltd. https://doi.org/10.1002/9780470727102

Shaffer, F., Gopalan, B., Breault, R. W., Cocco, R., Karri, S. B. R., Hays, R., & Knowlton, T. (2013). High speed imaging of particle flow fields in CFB risers. *Powder Technology*, 242, 86– 99. https://doi.org/10.1016/j.powtec.2013.01.012

Shao, Y., & Dong, C. H. (2006). A review on East Asian dust storm climate, modelling and monitoring. *Global and Planetary Change*, 52(1– 4), 1– 22. https://doi.org/10.1016/j.gloplacha.2006.02.011

Sweeney, M. R., & Valentine, G. A. (2017). Impact zone dynamics of dilute mono- and polydisperse jets and their implications for the initial conditions of pyroclastic density currents. *Physics of Fluids*, 29(9), 093304. https://doi.org/10.1063/1.5004197

H. Tennekes, & J. L Lumley. (Eds.). (1972). *A first course in turbulence* (Vol. 58, 816 pp.). Cambridge, MA: MIT Press. https://doi.org/10.1017/S002211207321251X

Tsuji, Y., & Morikawa, Y. (1982). LDV measurements of an air-solid two-phase flow in a vertical pipe. *Journal of Fluid Mechanics*, 120, 385– 409. https://doi.org/10.1017/S0022112084000422

Turnbull, B., & McElwaine, J. N. (2007). A comparison of powder-snow avalanches at Vallée de la Sionne, Switzerland, with plume theories. *Journal of Glaciology*, 53(180), 30– 40. https://doi.org/10.3189/172756507781833938

Valentine, G. A., & Sweeney, M. R. (2018). Compressible flow phenomena at inception of lateral density currents fed by collapsing gas-particle mixtures. *Journal of Geophysical Research: Solid Earth*, 123, 1286– 1302. https://doi.org/10.1002/2017JB015129